PCCP

ROYAL SOCIETY OF CHEMISTRY

PAPER

View Article Online
View Journal | View Issue

Cite this: *Phys. Chem. Chem. Phys.*, 2025, **27**, 24350

Towards elucidating the solar instability of the anti-fungal food preservative natamycin: insights from spectroscopy

Natasha J. Wrathall, [a] Jacob Eller, [b] Jake E. Barker, [a] Natércia d. N. Rodrigues, [c] Rachel K. O'Reilly, [a] Nicholas D. M. Hine [b] and Vasilios G. Stavros *[a]

Received 11th August 2025,
Accepted 27th October 2025

DOI: 10.1039/d5cp03071d

rsc.li/pccp

Natamycin, a natural antifungal peptide, is widely used in food and medicine. The absorption of natamycin in the ultraviolet region of the electromagnetic spectrum, is attributed to the conjugated linear chromophore present in the molecule. Upon irradiation, natamycin degrades, disrupting its antifungal efficacy. In an effort to understand these photodegradation pathways, the present study uses steady-state, transient electronic absorption and fluorescence lifetime spectroscopies allied with time-dependent density functional theory calculations to unravel the photodynamics of natamycin following absorption of ultraviolet radiation. We find that the photodynamics of natamycin are strongly influenced by the conjugated tetraene moiety, involving initial excitation to an optically bright ππ* state. The excited state population traverses a conical intersection into a second, optically dark, excited state from which it partially repopulates the ground state; the remaining excited state population leads to photoproduct formation. A photoproduct was isolated and characterised, and identified as being formed through a combination of isomerisation and epoxide ring-opening pathways. The insight garnered into the photodynamics of natamycin may facilitate design of next generation UV photostabilisers which protect natamycin against UV-induced degradation.

Introduction

Foods can become subject to fungal growth through storage and distribution, and many antimicrobial agents are therefore used to support in preservation of fresh produce.[1] Preservatives have been used for decades in the food industry, but there is now high demand for natural alternatives due to discovered long-term effects of artificial preservatives on health.[2–5] Consequently, research into the use of natural antimicrobial agents has intensified, which has motivated the present study.[6]

Natamycin (structure in Fig. 1), also known as pimaricin, is a naturally occurring antibiotic, containing an active tetraene moiety, that was isolated from the filtrate of a *Streptomyces natalensis* culture by Struyk *et al.* in 1955.[1,7] This tetraene group is reminiscent of 1,3,5,7-octatetraene, the photochemistry of which has been studied extensively.[8–13] Natamycin also has anti-mycotic properties which means it is used as a preservative in many commercially prepared food items such as yoghurt, sausages and cheese, to inhibit the growth of yeast and mould.[1,14–16]

Antifungal properties arise through natamycin's affinity to irreversibly bind to ergosterols which are present on the surface of fungi cells, thereby altering the permeability of the membrane and causing leakages of vital ions from the cell.[17] However,

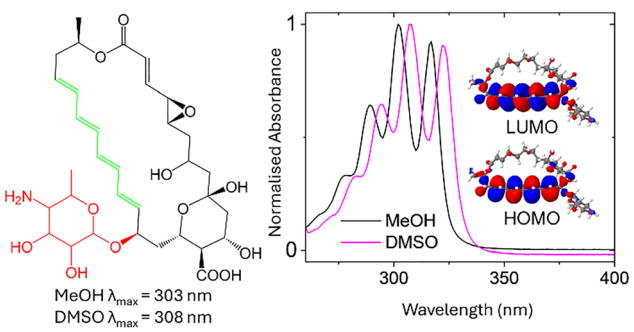

Fig. 1 Left: Structure of natamycin, highlighting the conjugated (green) and mycosamine (red) moieties with λ_{max} in methanol (MeOH) and dimethyl sulphoxide (DMSO) below. Right: The normalised absorption spectra for natamycin in MeOH (black) and DMSO (pink), with the highest occupied molecular orbital (HOMO) and lowest unoccupied molecular orbital (LUMO) for relaxed natamycin in implicit MeOH (right, inset).

[a] *School of Chemistry, University of Birmingham, Edgbaston, B15 2TT, UK. E-mail: v.stavros@bham.ac.uk*
[b] *Department of Physics, University of Warwick, Coventry, CV4 7AL, UK*
[c] *IBB-Institute for Bioengineering and Biosciences, Instituto Superior Técnico, Universidade de Lisboa, 1049-001, Lisboa, Portugal*

unlike its artificial counterpart, sodium benzoate, natamycin can be used in fermented goods as it does not interfere with bacterial growth, since ergosterol is not common in bacterial cells.[4,7] Low solubility in water means that natamycin typically sits on the surface of products, or requires complexing (usually with cyclodextrins) to enhance its solubility and stability.[18–20]

The stability of natamycin is highly dependent on its environmental conditions: the molecule is thermostable up to temperatures of ~100 °C and at pH 3–9, but photodegrades rapidly when exposed to ultraviolet (UV) light.[21–24] Foods treated with natamycin can be stored in darkness during their initial transportation; however, exposure to UV light is inevitable on supermarket shelves, which causes complete degradation within ~100 minutes.[25] Despite its rapid photodegradation, natamycin is still widely used to protect fermented foods which rely on bacteria, usually in combination with other preservatives to prevent microbial growth.[4,7]

While studies have shown that natamycin is unstable under UV irradiation (*i.e.*, it photodegrades), little is known about the photodynamical processes that underpin its photodegradation. Understanding how excess energy is dissipated by natamycin following the absorption of UV radiation could provide insight into potential strategies for its stabilisation. Controlled photodegradation could be achieved by altering natamycin's molecular structure to favour photodynamical mechanisms which avert excited state chemistry.[25] Slowed deterioration of the antifungal coating could in turn decrease the volume of food waste created by retailers and consumers, representing a significant economic and ecological impact.

Natamycin is well known for its solubility issues, therefore natamycin was studied in only two solvents: methanol (MeOH) and dimethyl sulphoxide (DMSO).[18–20] The choice of these two solvents was motivated by understanding how vastly different solvent environments (see below) affects the photodynamics, and hence long-term stability of the molecule. Only DMSO showed reasonable signs of solubility, serving as a nice comparison for our photodynamics studies of natamycin in both polar protic and polar aprotic solvents. It was not possible to perform any of the studies in a nonpolar aprotic solvent.

A multipronged approach was taken to unravel how the photoexcited state population evolves in natamycin upon UV irradiation. Ultrafast (femtosecond (fs) to nanosecond (ns)) spectroscopy was used to track the photodynamical processes, with steady-state absorption and emission being used to underpin the findings. Time-dependent density functional theory (TD-DFT) was also used to explicate the experimental findings. Additionally, structural analysis was undertaken of a photoproduct formed through solar irradiation in MeOH to try better to understand the photodegradation of this antifungal medication.

Results

Experimental

Two solvent environments were used in the study: MeOH and DMSO, which are polar-protic and polar-aprotic, respectively. The UV-Visible (UV-Vis) absorption spectra for natamycin in MeOH and DMSO are presented in Fig. 1. The absorption spectra for natamycin were comparable to those reported in the literature, with strong vibronic structure (*viz.* three peaks) characteristic of conjugated polyenes.[17,23] The red-shifted peaks in DMSO are expected due to MeOH's greater polarity.[26]

Each solution of natamycin was irradiated under a solar simulator and absorption spectra were recorded at different time intervals, up to 90 minutes (5400 seconds); further details are presented under experimental methods (below). Fig. 2 shows the resulting absorption spectra of natamycin in both MeOH and DMSO, indicating near complete photodegradation of natamycin in less than 90 minutes in both solvents. When dissolved in MeOH, the spectra show a reduction of absorbance in the vibronic bands (290–320 nm) and the appearance of new well-defined vibronic bands at a shorter wavelength (260–290 nm, >600 nm). The presence of vibronic bands in this region suggests conjugation is retained following irradiation, the product of this degradation is investigated below. However, for the solution of natamycin in DMSO, the spectra in Fig. 2 display a continual reduction of absorption with irradiation time, likely indicative of photoproduct formation, with evident loss of conjugation. Further irradiation experiments, involving narrow spectral-width irradiation (centred at the excitation wavelength of our ultrafast spectroscopy measurements) were carried out to furnish the findings *supra* and are presented in the SI. As with our solar simulator studies, we see similar spectral changes to those observed in Fig. 2. See SI for further details. To add, a spin-coated sample of natamycin on a CaF_2 window was also irradiated to try to mimic natamycin on the surface of foods; these data are also presented in the Fig. S3 (SI). The spin coated sample was too unstable to run any time-resolved measurements on, therefore it will not be discussed further.

To further investigate the photoproducts formed, a solution of natamycin was subjected to solar irradiation in methanol for 90 minutes before purifying *via* flash column chromatography. A comparison of FTIR spectra for the pre- and post-irradiated sample is shown in Fig. 3; further details are provided in the SI

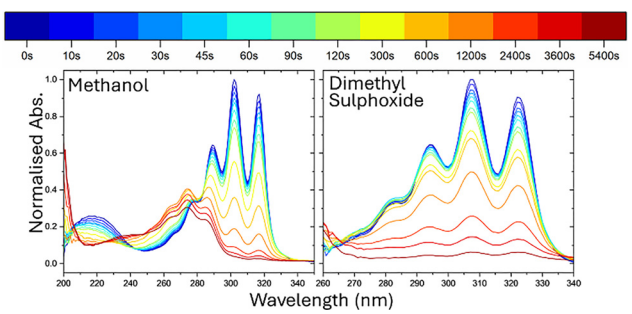

Fig. 2 UV-Vis absorption spectra of natamycin solutions dissolved in MeOH (left) and DMSO (right), at 10 μM in a 1 cm path length cuvette, at several time intervals after irradiation with a solar simulator. To note, the scale of the absorption spectra is different for MeOH and DMSO because of improper subtraction of the baseline in DMSO due to high absorption of the solvent.

including the NMR spectra of the pre- and post-irradiated sample (Fig. S4–S7, SI). Comparing the FTIR spectra seen in Fig. 3, the post-irradiated sample exhibits a general intensity decrease in the region 3750–2500 cm^{-1} and a new peak around 2981 cm^{-1} which is confirmed as a new hydroxyl group using NMR.[27,28] We also observe a loss of intensity in peaks between 1730 and 920 cm^{-1}, though the region appears to retain features corresponding to carbonyl groups, hydroxyl groups and alkene bonds. This signifies retention of these motifs but indicates a possible structural rearrangement. A noticeable peak reduction occurs at 1068 cm^{-1} which is assigned to the epoxide functional group undergoing a structural change.[29]

Considering the above, we hypothesise that under prolonged exposure to UV light, the epoxide can feasibly "ring-open" to a diol/alcohol-methoxy (due to the presence of methanol) species and thus would contribute to the appearance of –OH. This may explain the change in appearance of the peaks between 3750–2500 cm^{-1}. The reduction of peaks between 1730 and 920 cm^{-1}, and their broadening, could result from a ring-opened product. To note, several photoproducts were present in the sample, however, due to solubility issues, only one could be extracted and characterised. Whist full characterisation of these photoproducts is beyond the scope of this work, the above provides a plausible explanation for the appearance of a potential photoproduct. For further discussion on NMR characterisation, see NMR – SI.

Emission spectra of natamycin, dissolved in both MeOH and DMSO, were also obtained following photoexcitation at wavelengths corresponding to each of the vibronic maxima (see Fig. S8, SI). A similar emission profile was seen after excitation at each vibronic band. The quantum yield of fluorescence was found to be negligible (<0.1%). Emission lifetime measurements were also attempted for natamycin in MeOH and DMSO; these lifetime measurements were carried out in aerated samples and under nitrogen to ascertain whether emission could be originating from a triplet state (*i.e.*, *via* phosphorescence).[30,31] Our findings qualitatively suggest there is little-to-no observable difference between the air and N_2 measurements. The very low fluorescence quantum yields also precluded any reliable quantitative fitting of the emission lifetime data.

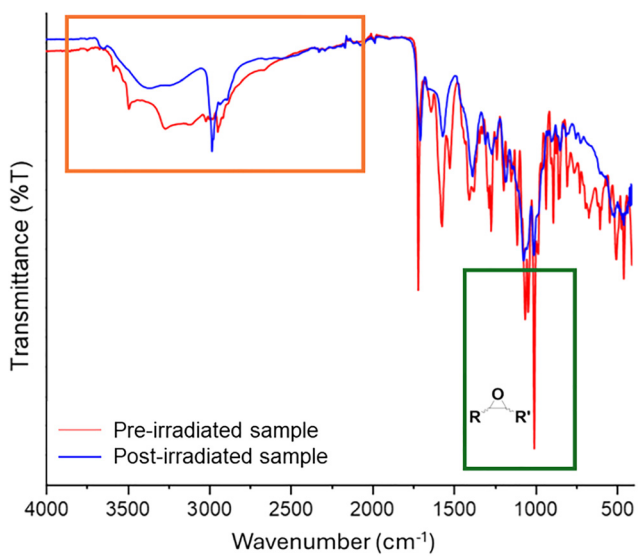

Fig. 3 IR spectra of both pre-irradiated (red) and the post-irradiated (blue) natamycin. The loss of the epoxide peak (green box) and the growth of a hydroxyl peak (orange box) is highlighted for clarity.

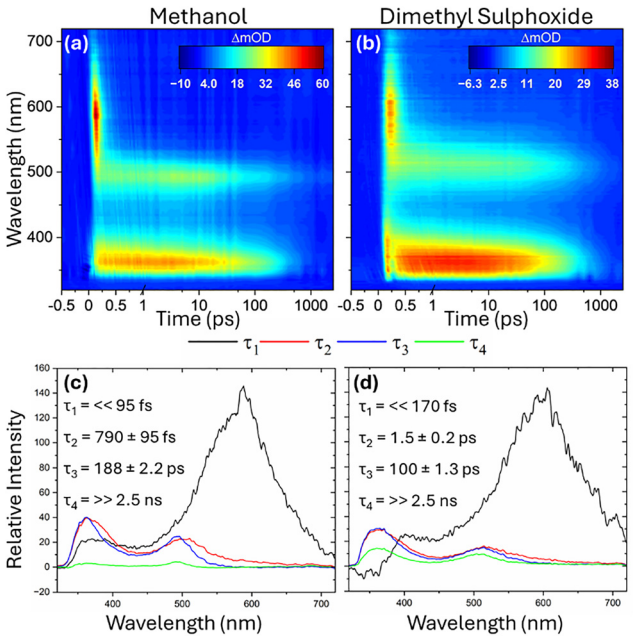

Fig. 4 TEAS presented as a chirp corrected false colour heatmap for natamycin in (a) MeOH and (b) DMSO excited at 303 and 307 nm, respectively. Evolution associated difference spectra (EADS) for natamycin in (c) MeOH and (d) DMSO with associated lifetimes (inset) extracted from a four-term global sequential fit.[32] EADS represent the evolving spectral features pertaining to each lifetime extracted and are labelled as such.

Transient electronic absorption spectroscopy (TEAS) of natamycin in MeOH and DMSO was carried out to explore the ultrafast photodynamics of the molecule, and to link these observations to the above-mentioned steady-state results. False-coloured heatmaps in Fig. 4a and b show TEAS data obtained for natamycin in MeOH and DMSO following photoexcitation at their λ_{max} (303 and 307 nm, respectively). The sample was photoexcited at several wavelengths corresponding to the peaks of each vibronic band (Fig. S10, SI), however no difference in the resulting photodynamics was seen, so the vibronic band with highest absorption is referred to hereafter. The short-lived (<170 fs) feature absorbing between 330–400 nm is present in DMSO-only measurements (*i.e.*, without natamycin) and is thus considered an instrument response of the experiment (see Fig. S11, SI). This short-lived component is not considered further.

Both heatmaps display equivalent spectral features, albeit decaying on different timescales: namely, a broad excited state absorption (ESA) containing several features (*vide infra*) between 500–700 nm. These ESA features have lifetimes less than the instrument response (95 and 170 fs for MeOH and DMSO, respectively). However, due to their absence in solvent-only scans (see Fig. S11, SI) they are attributed to photodynamics from the analyte. Following the fast decay of the

500–700 nm feature, two distinct ESA features at 350 and 500 nm extend for a few hundred picoseconds (Fig. 4a and b) and then narrow and persist beyond our experimental time-window (2.5 ns). Such a marked change in ESA can be attributed to the excited state population traversing onto a different electronically excited state. We return to discuss these features in more detail with the help of our TD-DFT calculations.

The TEAS data was fit using the Glotaran software package, implementing a global sequential fitting model.[32] The data was fit with four forward (pump–probe time delay > 0) exponential decay terms (see Fig. 4c and d). Evolution associated difference spectra (EADS) represent the evolving spectral features pertaining to each lifetime extracted (Fig. 4c and d) and are labelled as such. Associated residuals (Fig. S12, SI) were returned from the fitting procedure.[32] For completeness, equivalent TEAS data were obtained for solutions of natamycin at different concentrations to exclude any contributions from aggregates to the observed dynamics; the results of these experiments are presented in Fig. S13 (SI) and indicate no discernible concentration dependence on photodynamics.

TD-DFT calculations

In what follows, we refer to singlet adiabatic states and their corresponding potential energy surfaces (PESs) with two distinct nomenclatures (Fig. S14, SI). The conventional S_0, S_1, S_2, S_3 labels are assigned to states according to their energetic ordering at the Franck–Condon (FC) geometry. These labels are associated with the electronic structures of each assigned state, meaning the energetic ordering of labelled states changes when passing through conical intersections (CIs). Our alternative scheme labels the ground state and the first, second and third excited states with GS, ES1, ES2 and ES3, respectively. These labels reflect the energetic ordering of states across all of phase space; aside from seams of state degeneracy, the energetic ordering of these states is consistent. The use of this alternative scheme is motivated by the fact that the first, second and third excited states, as identified by single-point TD-DFT calculations, do not consistently correspond the states we have labelled as S_1, S_2, S_3, respectively, across all of phase space. Where necessary, calculations were carried out in implicit MeOH—no other solutions were studied theoretically. TD-DFT calculations predicted natamycin's lowest energy absorption between 363.3 and 361.6 nm (Table S2, SI), showing reasonable agreement with experimental data where the onset of absorption is $\sim$330 nm. The contribution of the ES2 $\leftarrow$ GS transition to the overall absorption spectrum is predicted to be negligible: for a group of independently relaxed conformers of natamycin, the oscillator strengths associated with these transitions are on average $\sim$0.032% of those associated with the ES1 $\leftarrow$ GS transition (Table S3, SI). The highest occupied molecular orbital (HOMO) and lowest unoccupied molecular orbital (LUMO) (Fig. S18, SI) are both predominantly situated on the conjugated chain moiety of the natamycin molecule (Fig. 1, highlighted in green). The ES1 $\leftarrow$ GS transition is almost purely (99%) HOMO $\leftarrow$ LUMO in character, and the associated transition density (Fig. S19, SI) confirms that charge redistribution upon electronic excitation to the ES1 almost exclusively occurs in this conjugated region. Hence, it is unsurprising that the relative peak positions and intensities observed in the UV-Vis absorption spectra shown in Fig. 1 are almost identical to those for 1,3,5,7-octatetraene.[8]

The GS relaxed conformers (Fig. S16, SI) are structurally very similar, with the all-*s-trans* tetraene moiety being present in all resulting structures. The only significant difference between the relaxed geometries is the dihedral angle between the mycosamine group and the remainder of the molecule (Fig. S15, SI). Despite this dihedral angle appearing to have little impact on the total energy of natamycin in the GS, the lowest energy conformer features a dihedral angle of 274.52°, and is hereafter referred to as the FC geometry. The low degree of variance in the predicted excitation energies obtained from independently relaxed geometries of different conformers of natamycin confirms that the peaks observed experimentally between 320 and 280 nm do not result from a mixture of conformer geometries. Instead, they make up the vibronic progression associated with the ES1 $\leftarrow$ GS transition. The spacing between the maxima of the two lowest energy peaks in the experimental absorption spectrum (Fig. 1) of natamycin in MeOH (1566.7 cm^{-1}/0.19425 eV) is assigned to a theoretically identified C=C stretching mode (Table S4 and Fig. S20, SI) within the linear tetraene moiety (1651.3 cm^{-1}/0.20474 eV), in agreement with the literature assignment of the infrared spectrum of 1,3,5,7-octatetraene.[11,33]

ES1 relaxations of GS relaxed geometries resulted in geometries that all feature the all-*s-trans* tetraene moiety (Fig. S17, SI). Akin to the GS relaxed geometries, the only significant structural difference between the conformers is the dihedral angle between the mycosamine group and the remainder of the molecule (Fig. S15, SI). Though, the ES1 relaxation of the three most energetically relevant GS relaxed geometries resulted in similar dihedral angles between 187.83° and 190.62°, giving the three lowest energy ES1 relaxed geometries. Hence, we expect the dominant ES1 relaxed geometry to be most accurately represented by these geometries We calculated fluorescence energies (Table S5, SI) for all ES1 relaxed geometries (Fig. S17, SI): these are seen to correspond to dark transitions and their energies show poor agreement with experimental values (Fig. S8, SI, MeOH). Thus, we expect that negligible fluorescence occurs from a minimum local to the FC geometry following ES1 $\leftarrow$ GS excitation. Further investigation identified a region of phase space accessible from the FC geometry in the ES1, with a bright ES1 $\leftarrow$ GS transition falling within the experimentally predicted wavelength range (identification of fluorescing geometries, SI). However, total fluorescence has been experimentally shown to be very weak, so emission from these conformers is still a relatively insignificant pathway.

Phosphorescence stemming from intersystem crossing (ISC) in the vicinity of the ES1 potential well local to the FC point, was also predicted to be insignificant. While the energies of the ES1 and T_2 states were within 3.6 meV of one another (Table S6, SI), suggesting there would be sufficient overlap of vibrational states, all spin–orbit coupling terms between the states were

~ 0 cm^{-1} in all directions (Table S7, SI). This is also corroborated experimentally by the absence of emission increase from solutions of natamycin under a nitrogen atmosphere (see above).

To investigate the feasibility of relaxation *via* internal conversion (IC) pathways, TD-DFT calculations were performed which indicated an ES1/ES2 conical intersection (CI) along the relaxation trajectory of natamycin (in MeOH) in the ES1. By examining the structural changes during the relaxation process, as determined by solvated geometry optimizations of the FC geometry in the ES1, we can decompose the relaxation into two main components: rotation of the mycosamine group (Fig. 1, red), and reorganization of the rest of the molecule. The ES1 and ES2 PES were traced (Fig. 5) across incremental rotations of the mycosamine group, from the dihedral angle in the FC geometry to the dihedral angle found in the ES1 local minimum proximal to the FC geometry. The surfaces are observed to nearly intersect as the dihedral angle decreases: the energy gap between them falls from $\sim$0.187 eV at 274.52°, to 0.084 eV at 189.02° (Fig. 5). This suggests that a nonadiabatic transition at an ES1/ES2 CI, causing the system to remain in the ES1 ($S_1 \rightarrow S_2$), is plausible following the initial ES1 $\leftarrow$ GS transition.

Discussion

Natamycin photodegrades rapidly, as seen in the solar irradiation studies in Fig. 2. Consequently, the majority of natamycin's relaxation trajectory after photoexcitation must include a pathway (or pathways) leading to degradation. Though it is difficult to definitively identify a single degradation pathway due to the complexity of the molecule, a viable initial relaxation trajectory, *en route* to degradation, has nevertheless been proposed. The calculations were only run in MeOH; hereafter, lifetimes and photodynamical pathways discussed therefore refer to natamycin in MeOH only.

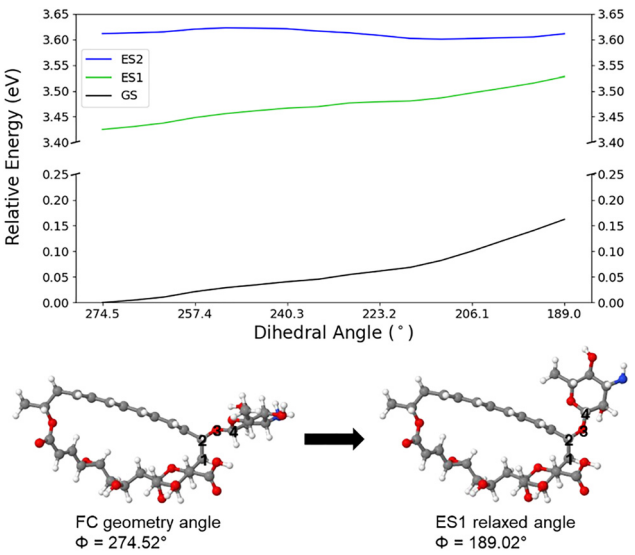

Fig. 5 Relative GS, ES1 and ES2 energies as a function of the dihedral angle (ϕ) involving atoms 1–4. Energies are relative to the GS energy where ϕ = 274.52°. Dihedral angles were scanned between 274.52° and 189.02° through rotation of the mycosamine group, approximating the relaxation trajectory from the FC geometry of natamycin (in MeOH) in ES1.

TD-DFT predictions of oscillator strengths (Table S3) found that photoexcitation at the wavelengths used in this study (303 nm for natamycin dissolved in MeOH) corresponds to a S_1 ($\pi\pi^*$) $\leftarrow$ S_0 transition. Following excitation to the S_1 state, the first lifetime (τ_1) is assigned to fast IC through a CI to the close-lying S_2 state discussed above. The movement of the population through the S_1/S_2 CI can be seen through the shifting ESA peaks in both the TEAS and, more evidently, the EADS (*viz.* Fig. 4c and d, black line). Our TD-DFT calculations also support the existence of a S_1/S_2 CI along the immediate relaxation trajectory of this system (Fig. 5). In support of this assignment, the corresponding τ_1 (black line) in Fig. 4c and d displays a substantially different spectral feature to τ_{2-4} (red, blue and green lines respectively), implying a large change in electronic structure. Within this lifetime, in addition to movement through the S_1/S_2 CI, solvent rearrangement and vibrational redistribution may also contribute.[33] Due to this lifetime being faster than the IRF extracted from our solvent scans (Fig. S11, SI), deconvolving the difference photophysical processes is not possible. Hence, the lifetime for τ_1 is quoted as less than our IRF ($\ll$95 fs). To add, the 500–700 nm feature is absent in the solvent-only response (Fig. S11, SI), and we can confidently attribute this to the analyte.

The second lifetime, τ_2 (790 fs), is assigned to vibrational relaxation along the S_2 PES after traversing the CI towards a local minimum. The slight narrowing and blue-shift of these features in Fig. 4c and d (red line) show the vibrational cooling of natamycin before a reduction in signal due to depletion from depopulation, corresponding to the subsequent lifetime τ_3 (188 ps, blue line); residual population trapped in the excited state is assigned a lifetime τ_4 ($\gg$2.5 ns, green line). As mentioned *supra*, both these features decay on the same lifetime, therefore the same chromophore is responsible.

Whilst we have not directly located a specific degradation pathway, the low emission intensity seen in each sample suggests nonadiabatic processes (which leads to ground state repopulation or degradation) must be in operation. For this, we must focus on the possibility of isomerisation within the molecule. With our TD-DFT calculations showing the ES1 $\leftarrow$ GS transition to be an almost pure ($\sim$99%) LUMO $\leftarrow$ HOMO transition (in geometries that have vibrationally relaxed along the ES1 PES, Fig. S17, SI), and both the HOMO and LUMO being located on the conjugated tetraene moiety (Fig. 1, highlighted in green), geometry changes leading to relevant degradation pathways must predominantly involve the movement of atoms within this conjugated chain. Hence, if present, it is likely that nonradiative deactivation mechanisms in natamycin would be similar to the well-studied geometry reorganisations that lead to CIs between the S_0 and an excited singlet state in all-*trans*-1,3,5,7-octatetraene (AT-octatetraene, Fig. S22), which we therefore review here.

Olivucci *et al.* computed minimum energy pathways across the 2^1A_g (S_1) and 1^1A_g (S_0) states of AT-octatetraene, evaluating a variety of adiabatic and nonadiabatic mechanisms.[11] They

suggested that the dominant relaxation mechanism initially involves overcoming an energy barrier, found to be ~0.26 eV by Christensen *et al.*,[12] to reach a transition state characterised by a kink formed between the 3rd, 4th and 5th carbon atoms, and a 73° C=C bond twist between the 3rd and 4th carbons (Fig. S22, SI). Using this transition state geometry as a starting point, Marian *et al.*[13] minimized the density functional theory (DFT) and multireference configuration interaction S_1–S_0 energy gap; they found that a partial Hula-twist[34,35] around the 4th carbon atom was the key motion facilitating the S_1/S_0 CI. Their results suggest that relaxation from this CI could result in a mixture of the *cis*, *trans*-1,3,5,7-octatetraene, 4-*s*-*cis*-1,3,5,7-octatetraene and AT-octatetraene isomers. Olivucci *et al.* also identified a second transition state with a significant (~77°) C=C bond twist between the first and second carbons, for which they predicted an associated 0.43 eV energy barrier. Using this transition state as a starting point, and the same methodology as mentioned previously, Marian *et al.* located another S_1/S_0 CI. They suggested that passage through this CI likely results in the formation of a mixture of 2-*s*-*cis*-octatetraene and AT-octatetraene.

Although these pathways of AT-octatetraene, and the similarities the polyene bears to vibronic spectra of natamycin, are strongly indicative of related nonradiative decay pathways for natamycin, further investigation is nevertheless required to determine whether these mechanisms really dominate the photochemistry of solvated natamycin.[8] Full nonadiabatic dynamics simulations with accurate *ab initio* methods of natamycin, particularly if explicitly solvated, would be computationally unfeasible. Though, future work harnessing machine-learned interatomic potentials (MLIPs) could play a role in making such simulations feasible at this scale.[36,37]

As depicted in Fig. 6 (through the labels A, B, C...), there are potentially multiple nonadiabatic processes in operation to account for τ_3 (and subsequently τ_4) following traversal of the S_1/S_2 CI in natamycin. In addition to the *trans* → *cis* isomerisation and *trans*,*trans*-isomer regeneration identified in AT-octatetraene, we propose two additional process which involves breakdown of molecular integrity leading to ring opening on the epoxide (*vide supra*). In addition, the low quantum yields of emission, combined with calculated (weak) spin–orbit coupling matrix elements (Table S7, SI), adds further credence to our proposal that nonadiabatic processes dominate in the excited state dynamics of natamycin, with minimal contribution from luminescence. Usually, the photoproduct would be seen as a positive feature in the EADS. However, due to these molecules (including isomers and epoxide ring-opening products) absorbing <300 nm (Fig. 2) the chromophores produced are outside of our experimental (spectral) window. Additionally, the proposed ring-opened epoxide photoproduct degrades upon further (prolonged) irradiation (Fig. 2) meaning this structure is also not photostable. Plausible structures of the epoxide ring-opening photoproducts seen at 260–290 nm (Fig. 2) can be seen in Fig. S23 (SI). Both candidates show an isomerisation of the conjugated backbone. It is possible that the natamycin undergoes both structural changes (*i.e.* isomerisation and ring-opening) as it relaxes back to the ground state. The isomerisation of the

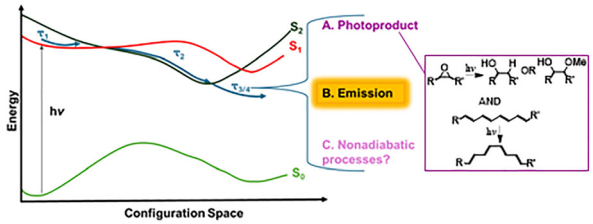

Fig. 6 Qualitative schematic of the overall relaxation dynamics of natamycin. The energy surfaces are labelled preserving their relative positions in the FC region. A, B and C indicate plausible relaxation mechanisms contributing to τ_3 and τ_4. The vertical line (labelled *hv*) corresponds to light absorbed.

conjugated region could account for any observed ESA features that we see in our TEAS data. Ultrafast isomerisation has been demonstrated in several different systems, as well as the isolated chromophore AT-octatetrene.[38–42] The epoxide ring opening is much less characterised on an ultrafast timescale; thus we cannot say with any certainty that the features we see in the TEAS are definitive evidence of this reaction taking place.[43,44]

As mentioned above, these two ESA features both decrease in intensity at the same rate, showing that the signals reflect depopulation of a single excited state. Aligning with the emission lifetime data, the final lifetime (τ_4), is assigned to the residual population fluorescing from a region of phase space where the ES1 ← GS transition is bright (identification of fluorescing geometries, SI).

Methods

Experimental set-up

To test the photostability of natamycin (purchased from Sigma-Aldrich, used without further purification), two separate 10 μM solutions were prepared with either MeOH, ethanol or DMSO, with 2 minutes of sonication to enhance dissolution. Each of these samples was irradiated with an LCS-100 solar simulator (Spectra-Physics) calibrated to an irradiance of 'one Sun' (1000 W m^{-2}). To monitor sample degradation, UV-Vis absorption spectra were obtained at regular intervals from 0 to 5400 seconds. The spin coated sample was prepared using a 70 mM solution in MeOH. The solution was filtered to remove any undissolved sample and was spin coated (3000 rpm for 20 seconds).

The emission spectra of natamycin dissolved in MeOH, ethanol and DMSO was recorded using a Horiba FluoroLog-3 fluorescence spectrometer. Natamycin dissolved in MeOH and DMSO were made up to be ~0.1 absorbance at λ_{max} in a 1 cm pathlength quartz cuvette. Emission spectra were obtained for natamycin, photoexcited at wavelengths corresponding to the maxima of each vibronic band, with the bandwidth set at 5 nm. Fluorescence lifetimes were extracted with the same equipment following photoexcitation from a 318 nm NanoLED. Experiments were done both in air and under nitrogen, achieved by bubbling nitrogen gas through the sample for 5 minutes.

The emission quantum yield for natamycin in MeOH and DMSO at 0.1 absorbance was measured using an Edinburgh

Instruments FS5 spectrofluorometer with the SC-30 integrating sphere module. The excitation wavelength was set to the λ_{max} of natamycin, and a 1 cm pathlength quartz cuvette was used.

A summary of the transient electronic absorption spectroscopy (TEAS) setup is given here in brief; previous publications describe the experimental setup in further detail.[45,46] Laser pulses of 800 nm central wavelength and 12 W with a 1 kHz repetition rate were generated *via* a Ti: sapphire regenerative amplifier (Spectra-Physics, Dual Ascend Pumped Spitfire Ace) seeded by a Mai Tai (Spectra-Physics). The resulting laser beam was split into four beams of equal power; the one used in these experiments was 3.5 W. This beam was split once more: a 2.5 W fraction was used to generate the 'pump' pulses whose wavelength can be selected through use of an optical parametric amplifier (TOPAS-C, Spectra-Physics). The power of the pump pulse at the sample was selected, using a neutral density filter, as 0.5 mW. Out of the remaining 1 W beam, 5% was used to generate a white light continuum (the 'probe' pulse); this is generated by focusing 0.05 W of this second beam into a CaF_2 window which produces a supercontinuum covering a wavelength range of approximately 315–740 nm.

A gold retroreflector (in the probe beamline) mounted onto an automated translation stage generated the pump–probe time delay, which was varied during the experiment. Both laser pulses pass through the sample: the pump beam photoexcites the sample and, at differing time delays, the probe monitors the absorption spectrum. Once through the sample, the probe pulse is collimated, passed through an 800 nm filter, and focussed with a lens into a fibre-coupled spectrometer (AvaSpec-ULS1650F, Avantes, Apeldoorn, The Netherlands). Changes in optical density (ΔOD) were determined (eqn (S1), SI). A 1 mM solution of natamycin was passed through a flow cell (Demountable Liquid Cell, Harrick Scientific Products Inc., Pleasantville, NY, USA) containing two CaF_2 windows (2 and 1 mm) spaced at 950 μm; the solution was passed through the cell using a diaphragm pump (SIMDOS 02) from a 25 mL reservoir.

Kinetic information from the ultrafast data was analysed using the software package Glotaran which uses a global sequential fitting model $\left(A \xrightarrow{\tau_1} B \xrightarrow{\tau_2} C \xrightarrow{\tau_3} D \xrightarrow{\tau_4} E\right)$ to fit evolving spectral features producing corresponding EADS.[32] The TEAS data was chirp corrected to aid visual interpretation using the software package KOALA before plotting as a heatmap.[47]

TD-DFT calculations

Calculations were run using the ESTEEM python package as a workflow manager.[48,49] All *ab initio* calculations were performed using ORCA/5.0.2, a Gaussian basis *ab initio* quantum chemistry package.[50–53] The size of natamycin (94 atoms) precludes well-converged CI search with multireference wavefunction methods. However, we only seek approximate geometries of intersections between excited states (rather than between ground and excited states, which are poorly represented in DFT-based methods). Hence, linear response (LR-) TD-DFT methods, combined with range-separated functionals, can be expected to be accurate for ground and excited state properties. The PBE0 hybrid exchange–correlation functional, def2-TZVP Karlsruhe basis set and D3BJ dispersion correction were used for all TD-DFT calculations.[48,52–56] A Conductor-like Polarizable Continuum Model (CPCM) was used to implicitly represent the solvent environment surrounding natamycin.[57] For all implicit solvent calculations, the CPCM model was parameterised by a dielectric constant (ε = 32.63) and refractive index (n = 1.329) to represent MeOH. Unless otherwise specified, all vertical excitations were calculated in implicit MeOH. All geometry optimizations were carried out using the Broyden–Fletcher–Goldfarb–Shanno algorithm.[58,59]

The PubChem database provided seven low-energy conformers of natamycin, generated using OpenEye's OMEGA software.[54,60] These conformers were used as starting configurations and geometries resulting from their simulation are denoted natamycin 1–7. GS gas phase geometry optimizations were carried out on the starting conformers. GS geometry optimizations of those configurations resulting from the gas-phase relaxation were then performed in implicit MeOH. Vertical excitation energies (ES1 ← GS, ES2 ← GS and ES3 ← GS) were then calculated for all relaxed GS geometries; these values correspond to predicted wavelengths of absorption.[61] MACE-OFF is a foundation MLIP for organic compounds based on the MACE architecture.[61] It was trained on ~952 000 conformations of organic molecules which were evaluated using DFT with the ωB97M-D3BJ[9,10] exchange–correlation functional and the def2-TZVPPD[11,12] basis set, as implemented in the PSI4 software package.[56] A normal mode analysis was carried out for the FC geometry in the gas phase using MACE-OFF. The difference in energies associated with the two lowest energy vibronic peaks in the experimental absorption spectrum was used to calculate the energy gap between the corresponding vibrational states. For a vibronic transition to be non-negligible, the motion along the corresponding associated vibrational mode must modulate the transition dipole moment. Hence, the vibration must involve the movement of atoms in the region(s) of the molecule where charge redistribution occurs. Thus, all modes with energies within 0.0124 eV (100 cm^{-1}) of the experimental energy gap were visually assessed for vibrations primarily involving atoms in the region of the molecule with significant ES1 ← GS transition density. Only one of the inspected modes featured vibrations of the atoms in this region, and a corresponding 10-snapshot trajectory file was written. TD-DFT was used to investigate the extent of the coupling between this vibrational mode and the transition dipole moment by calculating the ES1 ← GS oscillator strengths along this trajectory in the gas-phase.

The geometries obtained in the initial gas phase geometry relaxations of natamycin 1–7 were used as starting configurations for ES1 gas-phase geometry relaxations. The resulting configurations then underwent a further geometry optimisation in the ES1, solvated by implicit MeOH. Vertical excitation energies (ES1 ← GS) were then computed for the resulting configurations; obtained values correspond to predicted

emission wavelengths where the natamycin system in the ES1 relaxes into and fluoresces from a local potential well. $T_n \leftarrow GS$ (where n = 1,2,3) spin-forbidden vertical excitation energies, as well as the spin–orbit couplings between the ES1 and T_n states, were calculated for those geometries obtained through ES1 optimizations in implicit MeOH. The resulting data corresponds to a scenario where the natamycin system in the ES1 relaxes into a local potential well and undergoes ISC.

To look for evidence of a CI along the relaxation trajectory of natamycin in MeOH, following the ES1 ← GS transition, we started with the FC geometry. We then applied incremental dihedral rotations (involving atoms 1–4 in Fig. 5) to the mycosamine moiety in 15 equal steps, transitioning from the FC geometry dihedral angle to the dihedral angle found in the corresponding ES1 implicit solvent relaxed geometry (Fig. S17, SI, Natamycin 2). Throughout this process, the C–O–C angle (involving atoms 2–4 in Fig. 5) was fixed at the value observed in the implicit solvent ES1 relaxed geometry. TD-DFT calculations of energies for the ES1 and ES2 states were carried out for all resulting geometries in implicit MeOH.

Conclusions

The early photodynamics of natamycin have been explored using a range of different spectroscopic techniques and computational methods. UV excitation promotes the ground state population to a local S_1 ($\pi\pi^*$) electronic state. The molecule vibrationally cools as it traverses the S_1 potential energy surface, reaching an S_1/S_2 conical intersection *via* the rotation of the mycosamine moiety, resulting in population of the S_2 state. From here, natamycin can either return to the S_0 state or undergo photochemistry, inferred through comparison to the all-*trans*-AT-octatetraene system and analysis of the IR spectra. Fluorescence decay to the ground state *via* a bright transition located along the S_2 PES, and a possible nearby triplet state is possible. However, the weak emission coupled to mild spin–orbit suggest neither pathway occurs with any appreciable yield.

One possible photoproduct of natamycin has been found through a combination of different techniques. These showed that two separate processes transpired: an epoxide ring opening exhibited through loss of peaks in IR and NMR spectra, and an isomerisation of the conjugated chromophore in line with previous observations for AT-octatetraene and with observed changes in structural spectra. Future work could involve transient vibrational absorption spectroscopy to delve into the possible degradation of the epoxide group; however, this may be challenging due to natamycin's poor solubility.

The results of this study indicate that stabilisation of natamycin may be possible by quenching the S_2 state. This could diminish the population capable of accessing a dissociation coordinate. To this effect, we are currently investigating the ultrafast dynamics of the complex formed between natamycin and cyclodextrins, which has been previously reported to, in part, photostabilise natamycin against UV radiation. Our studies will focus on the very early photodynamics of the complexation and how encapsulation improves the photostability of natamycin. By understanding this stabilising mechanism, it will assist in the further development of such UV stabilisers within the food industry, increasing the active window of natamycin and reducing food wastage.

Author contributions

N. J. Wrathall carried out the fs-TEAS, steady-state experiments and experimental analysis. J. Eller performed the computational calculations. J. E. Barker performed FTIR and NMR analysis of natamycin products. Manuscript drafts were reviewed and edited by Professors Rachel K. O'Reilly, Nicholas D.M. Hine and Vasilios G. Stavros, and Dr Natércia d. N. Rodrigues. The project was supervised by Professor Nicholas D. M. Hine and Professor Vasilios G. Stavros. N. J. Wrathall wrote the manuscript with input from all authors.

Conflicts of interest

The authors have no conflicts to declare.

Data availability

Computational data for this article is available *via* the Warwick Research Archive Portal (WRAP) at **https://wrap.warwick.ac.uk/192111/**. Additional raw experimental data is available upon request from the author.

Supplementary information (SI): further photostability studies, emission data, laser spectroscopy results and computational details. See DOI: **https://doi.org/10.1039/d5cp03071d**.

Acknowledgements

The authors would like to acknowledge Warwick Centre of Ultrafast Spectroscopy (https://warwick.ac.uk/*fac*/sci/wcus) for use of the Cary 60 UV/Vis Spectrometer, Horiba Fluorolog-3, and TA set-up and Dr Sopida Wongwas, Prof. Christophe Corre, and Dr Jack Woolley for discussions. N. J. W. would like to thank University of Birmingham for the studentship. J. E. acknowledges funding from the EPSRC CDT in Modelling of Heterogeneous Systems funded by EP/S022848/1. J. E. Barker would like to acknowledge the University of Birmingham for the award of a PhD studentship. Computing facilities were provided by the Scientific Computing Research Technology Platform of the University of Warwick using the High-Performance Computing (HPC) cluster Avon, and the Sulis Tier 2 platforms at HPC Midlands+ funded by the Engineering and Physical Sciences Research Council (EPSRC), grant number EP/T022108/1. V.G.S. thanks the Royal Society for a Royal Society Industry Fellowship.

References

1 L. R. Franssen, T. R. Rumsey and J. M. Krochta, *J. Food Sci.*, 2006, **69**, 347–350.
2 A. Gálvez, R. L. López, R. P. Pulido and M. J. G. Burgos, in *Food Biopreservation*, Springer, New York, NY, 1st edn, 2014, pp. 3–14.
3 J. O. Warner, *Arch. Dis. Child.*, 2024, **109**, 882–885.
4 Ł. J. Walczak-Nowicka and M. Herbet, *Nutrients*, 2022, **14**, 1497–1522.
5 K. Whelan, A. S. Bancil, J. O. Lindsay and B. Chassaing, *Nat. Rev. Gastroenterol. Hepatol.*, 2024, **21**, 406–427.
6 G. W. Gould, *Int. J. Food Microbiol.*, 1996, **33**, 51–64.
7 B. Callabero, P. Finglas and F. Toldra, *Encyclopedia of Food Sciences and nutrition*, Academic Press, Amsterdam, 2nd edn, 2003, vol. 1.
8 G. F. Woods and L. H. Schwartzman, *J. Am. Chem. Soc.*, 1949, **71**, 1369–1399.
9 E. R. Lippincott, W. R. Feairheller and C. E. White, *J. Am. Chem. Soc.*, 1958, **81**, 1316–1321.
10 S. Hirata, H. Yoshida, H. Torii and M. Tasumi, *J. Chem. Phys.*, 1995, **103**, 8955–8963.
11 M. Garavelli, P. Celani, N. Yamamoto, F. Bernardi, M. A. Robb and M. Olivucci, *J. Am. Chem. Soc.*, 1996, **118**, 11656–11657.
12 H. Petek, A. J. Bell, Y. S. Choi, K. Yoshihara, B. A. Tounge and R. L. Christensen, *J. Chem. Phys.*, 1992, **98**, 3777–3794.
13 I. Lyskov, H. Köppel and C. M. Marian, *Phys. Chem. Chem. Phys.*, 2017, **19**, 3937–3947.
14 M. Meena, P. Prajapati, C. Ravichandran and R. Sehrawat, *Food Sci. Biotechnol.*, 2021, **30**, 1481–1496.
15 J. Stark and S. Roller, *Natural antimicrobials for the minimal processing of foods*, Woodhead Publishing, Sawston, Cambridge, 2nd edn, 2013, pp. 82–97.
16 J. Delves-Broughton, C. A. Batt and M. L. Tortorello, *Encyclopedia of Food Microbiology*., Academic Press, Cambridge, MA, 2nd edn, 2014, pp. 87–91.
17 M. Szomek, P. Reinholdt, H.-L. Walther, H. A. Scheidt, P. Müller, S. Obermaier, B. Poolman, J. Kongsted and D. Wüstner, *Biochim. Biophys. Acta, Biomembr.*, 2022, **1864**, 184012–184029.
18 S. Fang, X. Peng, X. Liang, J. Shen, J. Wang, J. Chen and Y. Meng, *Food Biophys.*, 2020, **15**, 188–195.
19 E. M. M. Del Valle, *Process Biochem.*, 2004, **39**, 1033–1046.
20 J. Glisoni, D. A. Chiappetta, A. G. Moglioni and A. Sosnik, *Pharm. Res.*, 2012, **29**, 739–755.
21 H. Brik, *J. Antibiot.*, 1976, **29**, 632–637.
22 H. Brik and H. J. Brittain, *Analytical Profiles of Drug Substances and Excipients*, Academic Press, Cambridge, MA, 1981, vol. **23**, pp. 339–419.
23 J. L. Koontz, J. E. Marcy, W. E. Barbeau and S. E. Duncan, *J. Agric. Food Chem.*, 2003, **51**, 7111–7114.
24 A. H. Nihad and M. Salami, *Clin. Pharmacol. Biopharm.*, 2017, **06**, 177–183.
25 M. Mascarenhas, P. Chaudhari and S. A. Lewis, *Adv. Ther.*, 2023, **40**, 3332–3359.
26 C. Reichardt, *Chem. Rev.*, 1994, **94**, 2319–2358.
27 W. Kaye, *Spectrochim. Acta*, 1954, **6**, 257–287.
28 (*a*) G. R. Fulmer, A. J. Miller, N. H. Sherden, H. E. Gottlieb, A. Nudelman, B. M. Stoltz, J. E. Bercaw and K. I. Goldberg, *Organometallics*, 2010, **29**, 2176–2179; (*b*) J. Chen and M. D. Soucek, *J. Appl. Polym. Sci.*, 2003, **90**, 2485–2499.
29 G. R. Fulmer, A. J. Miller, N. H. Sherden, H. E. Gottlieb, A. Nudelman, B. M. Stoltz, J. E. Bercaw and K. I. Goldberg, *Organometallics*, 2010, **29**, 2176–2179.
30 J. Strömqvist, A. Chmyrov, S. Johansson, A. Andersson, L. Mäler and J. Widengren, *Biophys. J.*, 2010, **99**, 3821–3830.
31 G. C. McBane, I. Burak, G. E. Hall and P. L. Houston, *J. Phys. Chem.*, 1992, **96**, 753–755.
32 J. J. Snellenburg, S. P. Laptenok, R. Seger, K. M. Mullen and I. H. Stokkum, *J. Stat. Softw.*, 2012, **49**, 1–22.
33 J. C. Owrutsky, D. Raftery and R. M. Hochstrasser, *Annu. Rev. Phys. Chem.*, 1994, **45**, 519–555.
34 R. S. Liu and G. S. Hammond, *Proc. Natl. Acad. Sci. U. S. A.*, 2000, **97**, 11153–11158.
35 R. S. Liu, *Acc. Chem. Res.*, 2001, **34**, 555–562.
36 S. W. Moon, S. Y. Willow, T. H. Park, S. K. Min and C. W. Myung, *J. Chem. Theory Comput.*, 2025, **21**, 1521–1529.
37 S. Axelrod, E. Shakhnovich and R. Gómez-Bombarelli, *Nat. Commun.*, 2022, **13**, 3451.
38 Y. Zhang, N. Liu, K. Niu, X. Wang, J. Yang, F. Lu, J. Chen and D. Zhong, *Sci. Adv.*, 2025, **11**, 9919.
39 D. Garg, A. N. Tarnovsky and J. Sivaguru, *J. Phys. Chem. A*, 2025, **129**, 3876–3885.
40 A. M. Cowden, R. Losantos, A. L. Whittock, B. Peñín, D. Sampedro and V. G. Stavros, *Photochem. Photobiol.*, 2023, **100**, 298–313.
41 T. T. Abiola, J. M. Toldo, M. T. do Casal, A. L. Flourat, B. Rioux, J. M. Woolley, D. Murdock, F. Allais, M. Barbatti and V. G. Stavros, *Commun. Chem.*, 2022, **5**, 141–150.
42 J. R. Ackerman, S. A. Forman, M. Hossain and B. E. Kohler, *J. Chem. Phys.*, 1984, **80**, 39–44.
43 D. Murdock, S. J. Harris, J. Luke, M. P. Grubb, A. J. Orr-Ewing and M. N. Ashfold, *Phys. Chem. Chem. Phys.*, 2014, **16**, 21271–21279.
44 A. Bhattacherjee, K. Schnorr, S. Oesterling, Z. Yang, T. Xue, R. de Vivie-Riedle and S. R. Leone, *J. Am. Chem. Soc.*, 2018, **140**, 12538–12544.
45 A. L. Whittock, T. T. Abiola and V. G. Stavros, *J. Phys. Chem. A*, 2022, **126**, 2299–2308.
46 L. A. Baker, M. D. Horbury, S. E. Greenough, F. Allais, P. S. Walsh, S. Habershon and V. G. Stavros, *J. Phys. Chem. Lett.*, 2015, **7**, 56–61.
47 M. P. Grubb, A. J. Orr-Ewing and M. N. Ashfold, *Rev. Sci. Instrum.*, 2014, **85**, 64104.
48 T. J. Zuehlsdorff, P. D. Haynes, M. C. Payne and N. D. Hine, *J. Chem. Phys.*, 2017, **146**, 124504.
49 M. A. Turner, M. D. Horbury, V. G. Stavros and N. D. Hine, *J. Phys. Chem. A*, 2019, **123**, 873–880.
50 F. Neese, *WIREs Comput. Mol. Sci.*, 2017, **8**, 1327.
51 F. Neese, *WIREs Comput. Mol. Sci.*, 2011, **2**, 73–78.
52 F. Weigend, *Phys. Chem. Chem. Phys.*, 2006, **8**, 1057–1065.

53 F. Weigend and R. Ahlrichs, *Phys. Chem. Chem. Phys.*, 2005, **7**, 3297–3305.
54 C. Adamo and V. Barone, *J. Chem. Phys.*, 1999, **110**, 6158–6170.
55 S. Grimme, S. Ehrlich and L. Goerigk, *J. Comput. Chem.*, 2011, **32**, 1456–1465.
56 A. Hellweg and D. Rappoport, *Phys. Chem. Chem. Phys.*, 2015, **17**, 1010–1017.
57 V. Barone and M. Cossi, *J. Phys. Chem. A*, 1998, **102**, 1995–2001.
58 R. Fletcher, *Comput. J.*, 1970, **13**, 317–322.
59 C. G. Broyden, *IMA J. Appl. Math.*, 1970, **6**, 76–90.
60 E. E. Bolton, J. Chen, S. Kim, L. Han, S. He, W. Shi, V. Simonyan, Y. Sun, P. A. Thiessen, J. Wang, B. Yu, J. Zhang and S. H. Bryant, *J. Cheminform.*, 2011, **3**, 31.
61 D. P. Kovács, J. H. Moore, N. J. Browning, I. Batatia, J. T. Horton, Y. Pu, V. Kapil, W. C. Witt, I.-B. Magdău, D. J. Cole and G. Csányi, *J. Am. Chem. Soc.*, 2025, **147**, 17598–17611.